JTTEE5 6:43-49

Thermal Fracture Mechanisms in Ceramic Thermal Barrier Coatings

K. Kokini, B.D. Choules, and Y.R. Takeuchi

Ceramic thermal barrier coatings (TBCs) represent an attractive method of increasing the high-temperature limits for systems such as diesel engines, gas turbines, and aircraft engines. However, the dissimilarities between ceramics and metal, as well as the severe temperature gradients applied in such systems, cause thermal stresses that can lead to cracking and ultimately spalling of the coating. This paper reviews the research that has considered initiation of surface cracks, initiation of interfacial edge cracks, and the effect of a transient thermal load on interface cracks. The results of controlled experiments are presented together with analytical models. The implications of these findings to the differences between diesel engines and gas turbines are discussed. The importance of such work for determining the proper design criteria for TBCs is underlined.

Keywords diesel engines, edge cracks, gas turbines, interface cracks, thermal barrier coatings, thermal fracture

1. Introduction

HIGH-TEMPERATURE SYSTEMS such as diesel engines, gas turbines, and jet engines need the development, design, and use of materials that can make it feasible to leap to the temperature requirements of next-generation systems. Ceramic thermal barrier coatings (TBCs) offer an attractive means of protecting the current metallic components. On the other hand, the significant differences in properties between ceramic and metal, as well as the severe environments that these materials have to survive, present challenging scientific problems, because under these circumstances these systems tend to delaminate and spall. Many studies have considered the time to spalling under different conditions (Ref 1-3). One significant contributor to such spalling is oxidation of the bond coat in conditions that simulate jet engine applications (Ref 4, 5). However, even in diesel engines where conditions do not lead to oxidation, spalling has been found to limit the use of TBC (Ref 6). Consequently, there has been a more concentrated effort in recent years to study the mechanisms of crack initiation and propagation in TBCs under controlled experimental conditions. This paper reviews such efforts by the present authors and presents the results obtained with respect to surface crack initiation and the implications for using functionally graded materials systems. The differences between diesel engines and gas turbines/jet engines from the perspective of TBC design are shown. The results for edge crack initiation are also reviewed with similar conclusions.

2. Initiation of Surface Cracks

The objective of this work was to identify the mechanisms by which the first crack initiates on the surface of a multilayer, graded ceramic TBC. The experimental conditions were designed to simulate thermal loadings that are encountered in the combustion chamber of a diesel engine. The materials system used was one that was experimented with on the surface of a piston. The beam specimens shown in Fig. 1 were subjected to a concentrated line heat flux at the surface (Ref 7). The specimen was made of a steel substrate with a bond coat (CoCrAlY), a

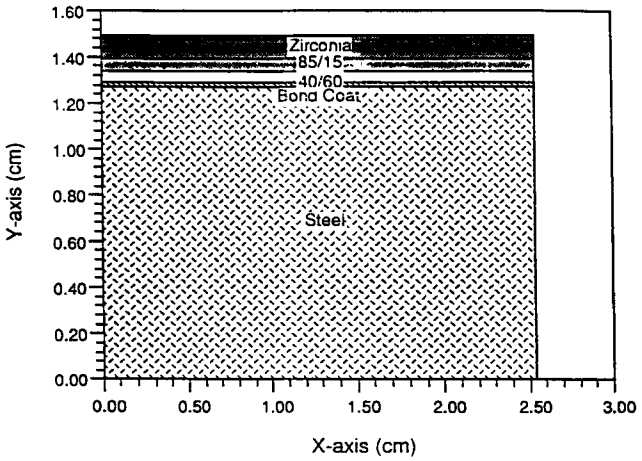

Fig. 1 One-half of beam-shaped specimen used for surface crack initiation studies

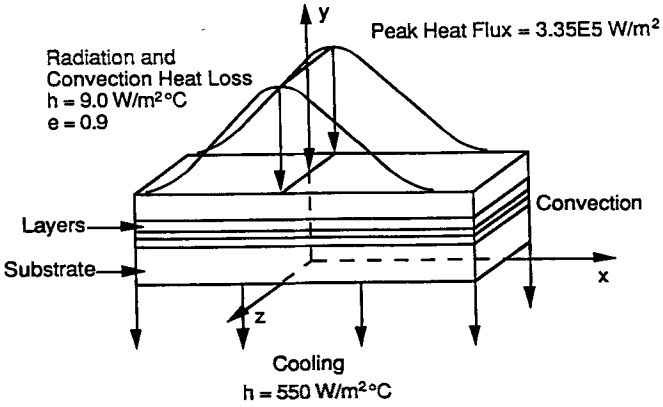

Fig. 2 Boundary conditions representing the thermal loading under the heat lamps

K. Kokini, B.D. Choules, and **Y.R. Takeuchi,** Purdue University, School of Mechanical Engineering, West Lafayette, IN 47907, USA.

0.508 mm (0.02 in.) thick layer of 40% zirconia with 60% bond coat, followed by a 0.508 mm (0.02 in.) thick layer of 85% zirconia/15% bond coat and, at the surface, a 1.016 mm (0.04 in.) thick layer of 100% zirconia. Figure 1 represents one-half the total length of the specimens used.

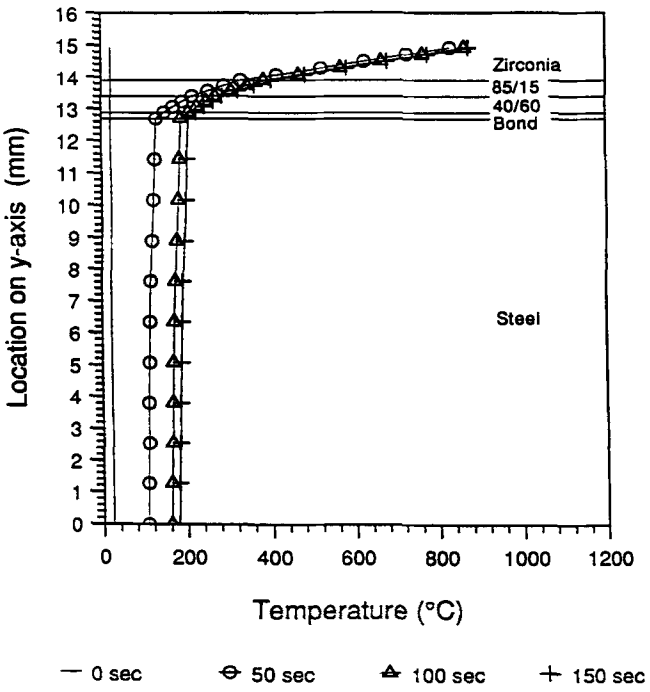

Fig. 3 Calculated temperature distribution in the specimen at different times

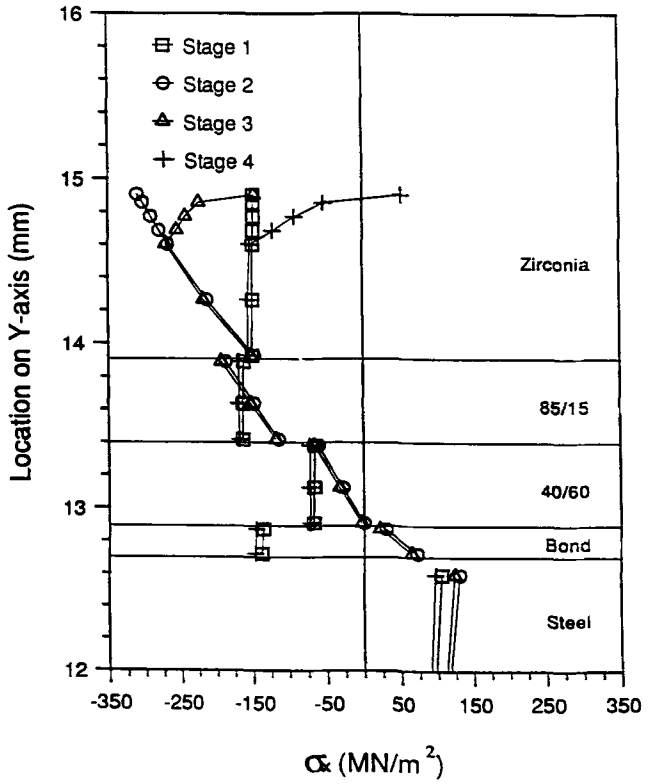

Fig. 4 Stress distribution across the coating/substrate profile. Stage 1: Residual stress. Stage 2: Steady-state heating. Stage 3: Stress relaxation for 2 h. Stage 4: Uniform cooling to room temperature

The experimental setup consisted of two high-intensity infrared focused lamps that projected a line heat flux at the center of the specimen. The bottom of the steel substrate was cooled by a water-cooled copper plate. The experimental boundary conditions are shown in Fig. 2. These conditions were obtained by performing detailed temperature measurements that were then fitted into a finite element model.

The experimental procedure consisted of subjecting the surface to the heat flux until steady-state conditions were reached, keeping it at steady state for 2 h, and then allowing it to cool to room temperature. The calculated temperature distribution caused by this thermal loading history is shown in Fig. 3. All such experiments resulted in crack formation at the surface (x = 0 in Fig. 1), in the region where the heat flux was concentrated (Ref 7). The stress distributions, calculated using the finite element method at the different stages of the thermal loading process, are shown in Fig. 4. The surface was under some residual in-plane compression due to an assumed uniform cooling from a manufacturing temperature of 590 °C. The application of the heat flux caused increased compression. However, this compressive stress was relaxed after 2 h at steady state, and when the specimen was cooled to room temperature a tensile stress was generated that is believed to have initiated the crack. This mechanism was confirmed by measuring the variation of strain at the bottom of the substrate in a different specimen configuration (Ref 8).

3. Initiation of Edge Cracks

In order to study the effect of a transient thermal load on the initiation of edge cracks in TBCs, the experiment described above was modified by allowing the line heat flux to be applied over the *length* of the specimen (Fig. 5). Also, in order to significantly decrease the effect of stress relaxation, the coating was made of multiple layers of mullite instead of zirconia (Fig. 6). Besides its reduced stress relaxation behavior, mullite exhibits a lower thermal expansion coefficient than zirconia. As a result, when water cooling was applied at the bottom of the substrate, it was not possible to obtain any cracking. Thus, the experimental procedure was modified by removing the water cooling and allowing the substrate to be exposed to air. The control of the thermal loading (and therefore of the stresses) was then provided by controlling the time of heating and applying convective surface cooling with the help of an air jet. A typical example of the temperature-time history for the surface and substrate is shown in Fig. 7. These calculated temperature values match experimentally measured ones. The corresponding in-plane stress versus time, calculated at the center of the surface of the coating, is shown in Fig. 8.

At the end of the heating process (t = 120 s), the surface was under a small tensile stress. When the air jet cooling was activated at the same instant, a significantly larger transient maximum tensile stress was obtained. If further heating had been allowed, the stresses would have reached the same level of tension without the cooling, because as the temperature in the specimen became more uniform with time, the substrate would have expanded more than the surface, causing a tensile stress to

develop. The transient peak stress during cooling is plotted in Fig. 9 as a function of the temperature difference between the coating surface (T_c) and the substrate (T_s) for different values of T_c, at the instant when the heating is terminated and the cooling is initiated. This shows that as T_c increases, the surface stress increases. Similarly, as ($T_c - T_s$) decreases, the stress also increases. Therefore, for applications such as diesel engines, where the surface temperature is relatively low (~800 °C) and the temperature difference ($T_c - T_s$) is relatively large due to aggressive cooling, mullite is an excellent alternative to zirconia in terms of durability, at least as measured by stresses resulting from differential thermal expansion of the cracking and substrate. However, for a jet engine application, where T_c is large and ($T_c - T_s$) is small, the same material would result in significant surface cracking.

The behavior of the edge of the interface is impossible to quantify in terms of stresses, because these become singular at the edge (Ref 9). Consequently, these stresses are expressed in terms of quasi-stress intensity factors K_1 (opening mode) and K_2 (shearing mode) as:

$$\sigma_{yy} = K_1 r^{-\beta} \quad \text{(Eq 1)}$$

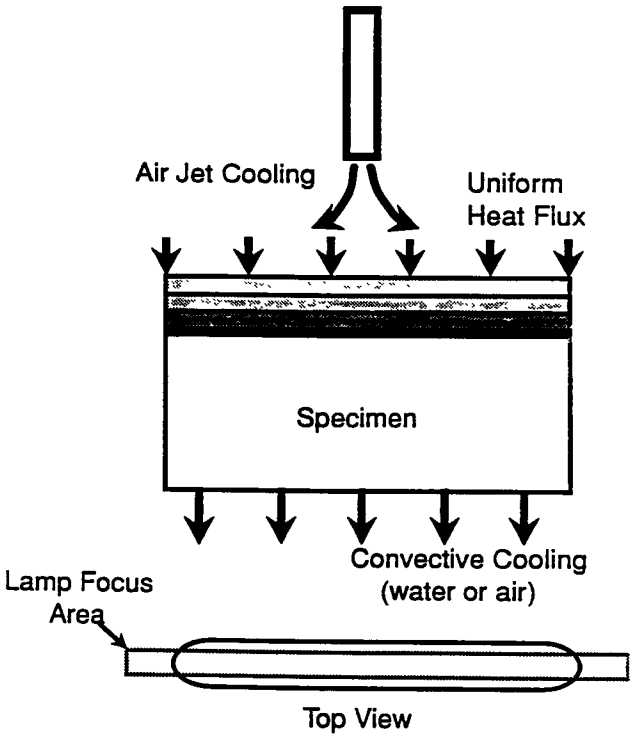

Fig. 5 Schematic of side view and top view of beam specimen and the applied thermal loading for edge crack initiation experiments

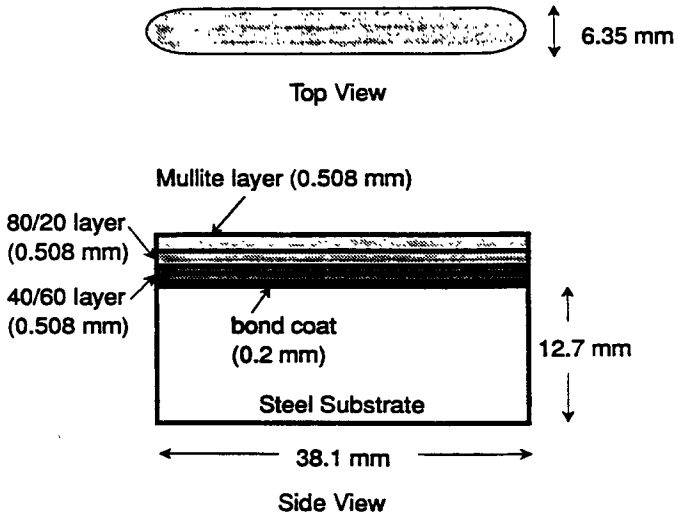

Fig. 6 Beam specimen used for edge crack initiation studies

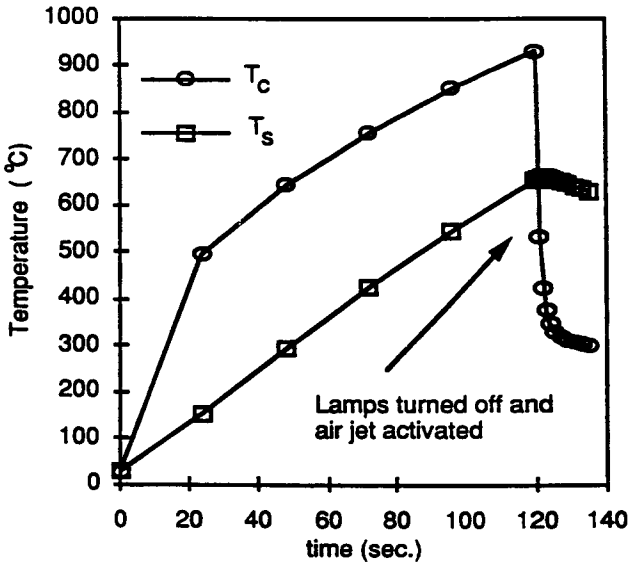

Fig. 7 Calculated temperature vs. time for coating surface and substrate

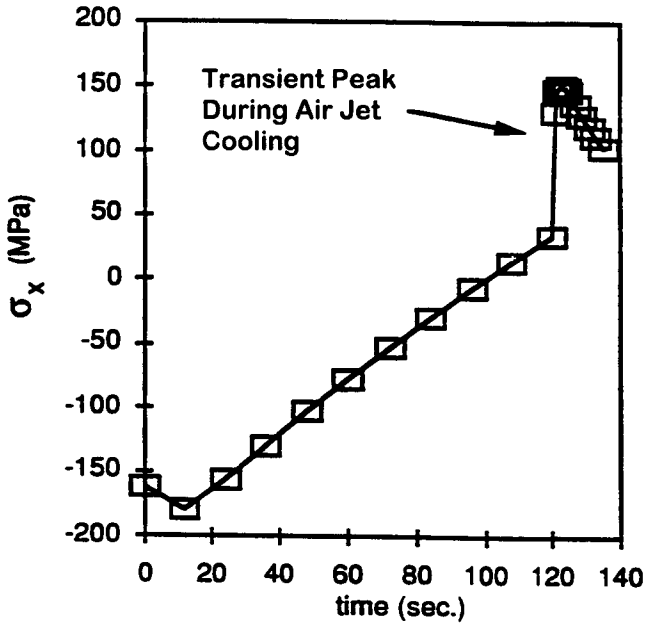

Fig. 8 Surface stress at the center of the beam specimen shown in Fig. 6 vs. time

$$\sigma_{xy} = K_2 r^{-\beta} \quad \text{(Eq 2)}$$

where σ_{yy} and σ_{xy} are respectively the stress component normal to the interface and the shear stress component. The parameter r represents the distance from the free edge, while β is an exponent that quantifies the strength of the singularity. β is dependent on the Young's moduli, the Poisson's ratios of the two materials, and the geometry of the edge of the interface. The details of the calculations related to determining K_1 and K_2 when subjected to a transient thermal load are presented elsewhere (Ref 10). In general, the time-dependent behaviors of K_1 and K_2 are similar to that of the surface stress when subjected to the transient thermal load. Therefore, in Fig. 10(a) and (b) the values of the maximum K_1 and K_2, respectively, at the edge of interface 3 are plotted versus $(T_c - T_s)$ for different values of T_c. For both quantities the magnitudes are largest when T_c is large and $(T_c - T_s)$ is small.

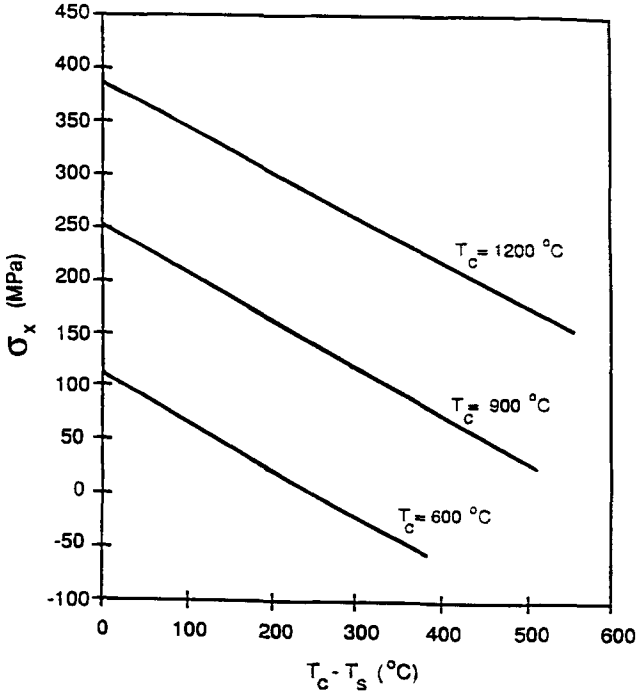

Fig. 9 Maximum surface stress at the center of the beam specimen shown in Fig. 6 vs. $(T_c - T_s)$

In Fig. 10, the values of K_1 and K_2 at interface 3 are given because the experiments showed that crack initiation always occurred at the 60/40 bond coat interface. This is also the interface that experiences the largest magnitude of K_1. In general, reducing the magnitudes of K_1 and K_2 should reduce crack initiation at the edge. Figure 10 shows again that thermal loading conditions encountered in an aircraft engine would be detrimental to the edge compared to conditions in a diesel engine.

4. Initiation of Interface Cracks

An interesting aspect of thermal fracture mechanisms of TBCs is cracking of one of the interfaces between any of two layers in a multilayer material system. In particular, the question of which interface is most likely to exhibit crack initiation and how to predict it is a challenging one. In order to develop some understanding of the mechanics of such processes, a model was

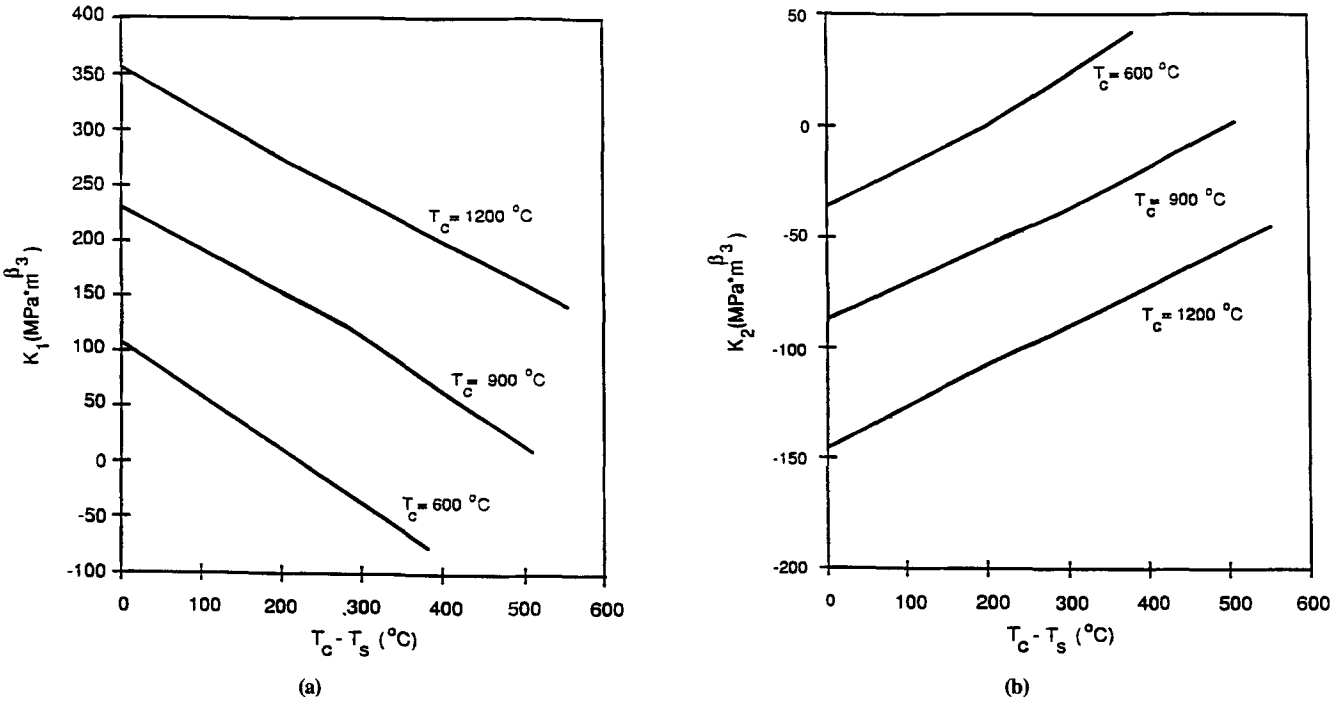

Fig. 10 (a) Maximum K_1 vs. $(T_c - T_s)$ for interface 3 of the beam specimen shown in Fig. 6 ($\beta_3 = 0.0049$). (b) Maximum K_2 vs. $(T_c - T_s)$ for interface 3 of the beam specimen shown in Fig. 6 ($\beta_3 = 0.0049$)

used that considered the presence of an interface crack of length $a = 0.3175$ mm between the top layers (Fig. 11). The cases of a zirconia coating and a mullite coating were considered.

The model was used to simulate the effect of applying a transient thermal load at the surfaces due to a heat flux generated by high-intensity infrared lamps or a high-power (1.5 kW) CO_2 laser. The distribution of the heat flux on the surface due to each method of heating is shown in Fig. 12. In Fig. 11 and 12, $x = 0$ shows the center of the specimen. Thus, the specimen and the heat flux are symmetric about $x = 0$. The sides and bottom of the specimen were cooled by free convection ($h = 5$ W/m$^2 \cdot$ K, $T_\infty =$ 300K). The specimen was heated for 3 min with the lamp and for 5 s with the laser. After the transient heating, the specimen was allowed to cool to room temperature.

The finite element software package ABAQUS (Hibbitt, Karlsson and Sorensen, Inc., Providence, RI) was used to model the specimen. Plane-strain, eight-node quadrilateral elements were used for the calculation of the transient temperature and stress distributions. The model assumed the crack to be insulated. From this model the transient opening (Δv) and shearing deformations (Δu) near the crack tip were calculated. This information was then used to calculate the transient strain energy release rate, G, due to the thermal load. The equations used for calculating G have been presented elsewhere and will not be repeated here (Ref 11, 12).

The measured surface temperature for both zirconia and mullite specimens are shown in Fig. 13. The calculated temperature distribution around the surface of the crack, immediately before cooling, is presented for each case in Fig. 14. It is clear that the assumption of an insulated crack results in a large temperature change across the crack.

The calculated crack openings Δv near the crack tip at a distance of $r = 7.94 \times 10^{-6}$ mm are presented in Fig. 15. The largest crack opening occurs for the mullite interface subjected to laser heating. Clearly the zirconia experiences a larger crack tip opening under laser heating than under the heat lamps. On the other hand, the largest crack tip shearing deformation shown in Fig. 16 is experienced by the zirconia interface subjected to laser heating. The resulting transient strain energy release rates shown in Fig. 17 indicate that the largest G is experienced by the zirconia coating subjected to laser heating followed by cooling. In particular, the laser heating should result in a significantly fa-

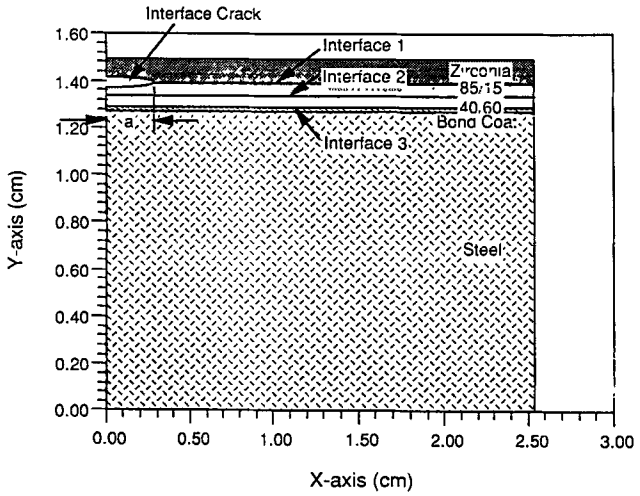

Fig. 11 Model of half a beam specimen used to study the behavior of an interface crack. ($y = 0$ is the bottom of the substrate and $x = 0$ is the center of the specimen.)

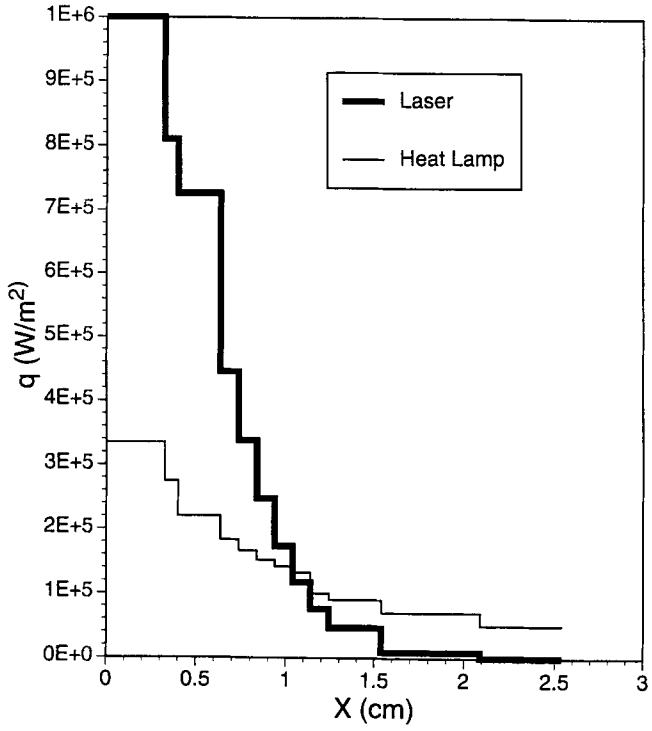

Fig. 12 Distribution of heat flux applied on the surface for interface crack

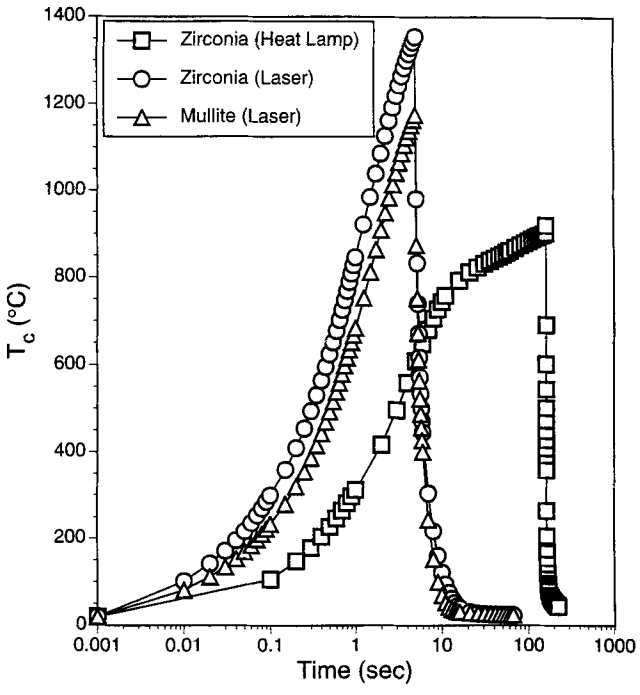

Fig. 13 Surface temperature at $x = 0$ vs. time for the different thermal loadings

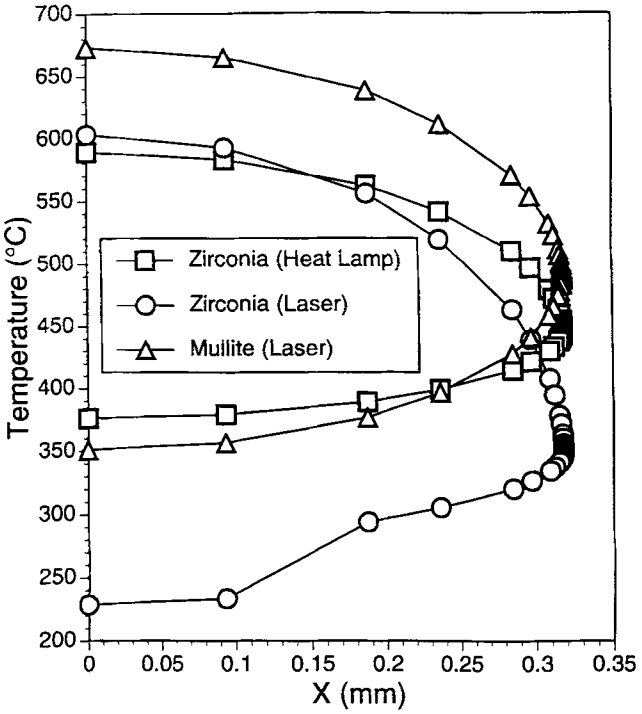

Fig. 14 Temperature distribution around the surfaces of the crack at the time of maximum surface temperature. ($x = 0$ is the center of the crack as shown in Fig. 11.)

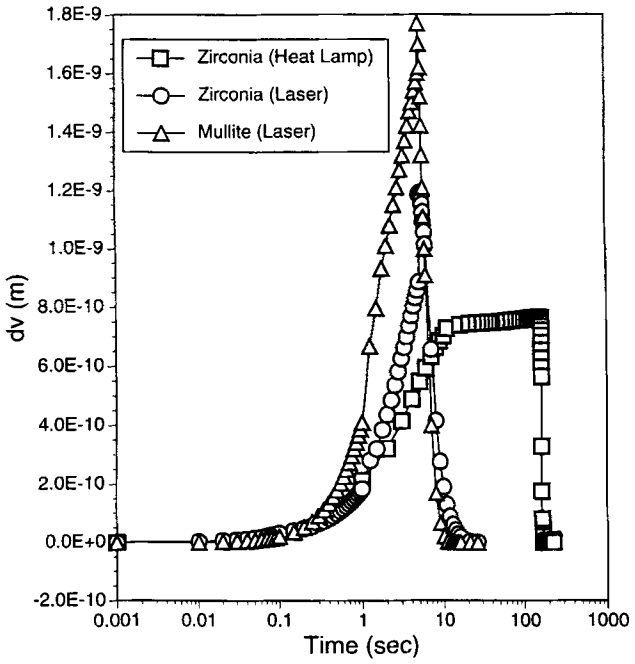

Fig. 15 Crack tip opening vs. time at $r = 7.94 \times 10^{-6}$ mm from the crack tip

cilitated interface crack propagation process compared to the infrared lamp heating. If it is therefore assumed that the laser heating simulates conditions similar to those encountered in a gas turbine/aircraft engine, delamination of the interface is expected to occur sooner in this system than in a diesel engine. On the other hand, it is possible that mullite could be more resistant than zirconia to such delamination. These predictions have not been verified experimentally and are the subject of ongoing investigations.

5. Conclusions

Ceramic TBCs are subjected to various transient thermomechanical loads during their use that result in different potential crack initiation and propagation mechanisms. The results presented above consider three mechanisms: surface cracking, free-edge cracking, and interface cracking.

Surface cracking is shown to initiate, in the case of zirconia coatings, from stress relaxation at high temperature, which decrease the compressive stresses due to heating over time and results in tensile stresses upon cooling. The use of a material such as mullite, which does not relax as much as zirconia, was shown to result in at least an order of magnitude increase in the life of the coating (Ref 13, 14). It was also shown that, while the mullite is an excellent substitute for zirconia in a diesel engine, the same would not be true in a gas turbine, because of the significantly different thermal loading conditions.

In the case of edge crack initiation, the results showed that the singular nature of the stresses does not allow a stress criterion to be used. The edge does experience both opening and shearing modes of stress intensity factors, which like surface stresses behave considerably differently in diesel engines and gas turbine environments.

The interface cracks subjected to different transient thermal loading conditions experience significantly different opening and shearing deformations, as well as different total strain energy release rates, G. The significance of each of these quantitative measures to crack propagation needs to be determined by experimental work, which is in progress.

It is clear, however, that the design of a TBC is a complex process that has to consider the thermal loading and other conditions that can be vastly different from one application to another. In each case, the design process needs to establish criteria for acceptability from the point of view of delaying crack initiation and propagation processes. On the other hand, since the function of a TBC is to protect metallic substrates from high temperatures, the thermal resistance of the coating is also an important consideration.

In recent years, the worldwide research efforts related to functionally graded material systems have offered additional design opportunities, while at the same time complicating the design equation (Ref 15, 16). It has been shown by the present authors, however, that a functionally graded coating can be designed which would resist surface cracking, as well as a very thin coating with an increased thermal resistance (Ref 17).

Acknowledgments

Support of this research by Cummins Engine Company and the National Science Foundation through Grant No. MSS 9301265 is gratefully acknowledged.

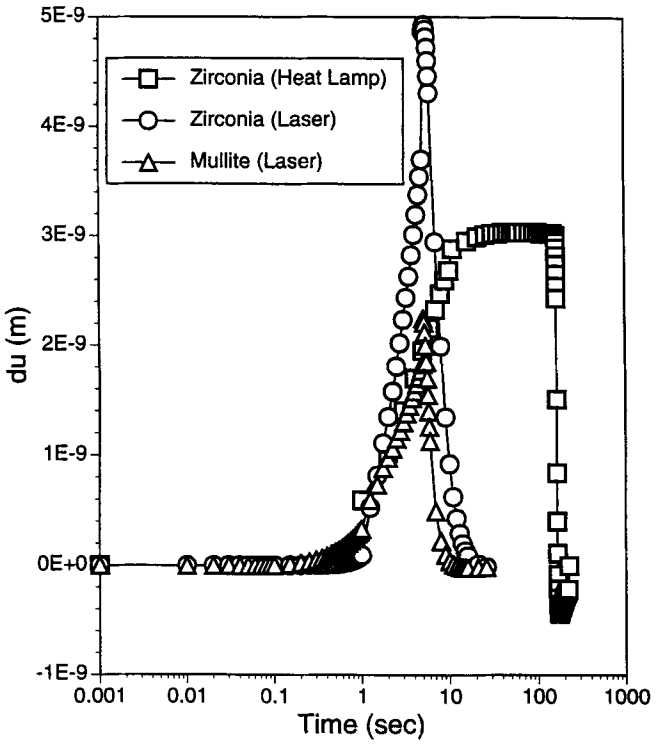

Fig. 16 Crack tip sliding vs. time at $r = 7.94 \times 10^{-6}$ mm from the crack tip

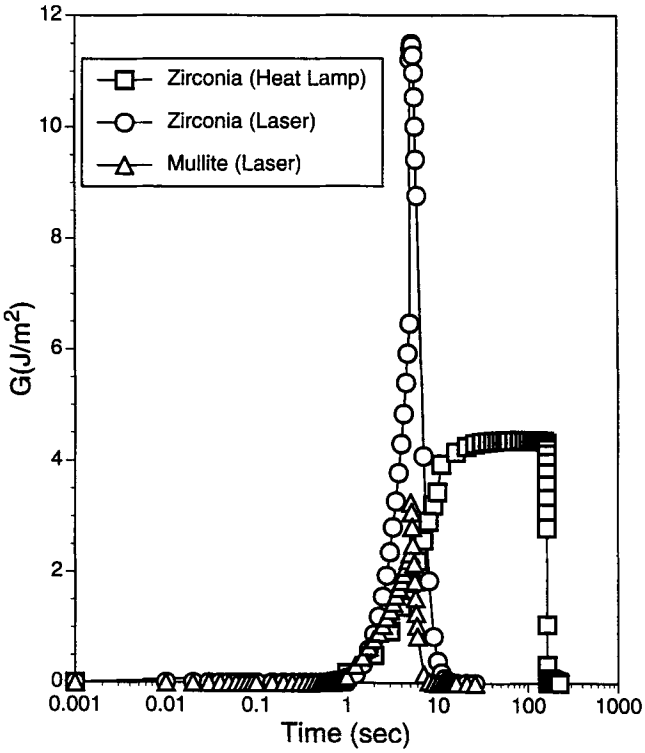

Fig. 17 Strain energy release rate vs. time

References

1. R.A. Miller and C.C. Berndt, Performance of Thermal Barrier Coatings in High Heat Flux Environments, *Thin Solid Films,* Vol 119, 1984, p 195-202
2. C.H. Liebert and R.A. Miller, Ceramic Thermal Barrier Coatings, *Ind. Eng. Chem. Prod. Res. Dev.,* Vol 12, 1984, p 334-349
3. J.T. DeMasi, K.D. Sheffler, and M. Ortiz, "Thermal Barrier Coating Life Prediction Model Development," NASA CR 182230, National Aeronautics and Space Administration, Dec 1989
4. R.A. Miller and C.E. Lowell, Failure Mechanisms of Thermal Barrier Coatings Exposed to Elevated Temperatures, *Thin Solid Films,* Vol 95, 1982, p 265-273
5. W.J. Brindley and R.A. Miller, Thermal Barrier Coating Life and Isothermal Oxidation of Low-Pressure Plasma-Sprayed Bond Coat Alloys, *Surf. Coat. Technol.,* Vol 43-44, 1990, p 446-457
6. T.M. Yonushonis, K.L. Hoag, P. Huston, A.P. Matarese, R.C. Novak, and D.P. Roehling, Thick Thermal Barrier Coatings for Diesel Engines, *Proc. 25th Automotive Tech. Dev. Contract. Coord. Mtg.,* Publication P2009, Society for Automotive Engineers, 1987
7. K. Kokini and Y.R. Takeuchi, Initiation of Surface Cracks in Multilayer Ceramic Thermal Barrier Coatings under Thermal Loads, *Mater. Sci. Eng. A,* Vol 189, 1994, p 301-309
8. Y.R. Takeuchi and K. Kokini, Thermal Fracture of Multilayer Ceramic Thermal Barrier Coatings, *J. Eng. Gas Turbines Power (Trans. ASME),* Vol 116, 1994, p 266-271
9. D.B. Bogy, Two Edge-Bonded Elastic Wedges of Different Materials and Wedge Angles under Surface Tractions, *J. Appl. Mech.,* Vol 38, 1971, p 377-386
10. M. Case and K. Kokini, Thermally Induced Initiation of Interface Edge Cracks in Multilayer Ceramic Thermal Barrier Coatings, *Proc. Symp. Ceramic Coatings,* K. Kokini, Ed., ASME MD, Vol 44, 1993, p 149-162
11. R.R. Reynolds and K. Kokini, Transient Thermoelastic Fracture of Interface Cracks: Effect of Bending Restraints, *Int. J. Fract.,* Vol 54, 1992, p 185-195
12. K. Kokini and Y.R. Takeuchi, Transient Thermal Fracture of an Interface Crack in the Presence of a Surface Crack, *J. Therm. Stresses,* Vol 17, 1994, p 63-74
13. Y.R. Takeuchi, K. Kokini, and T.M. Yonushonis, Thermal Barrier Coating Development for Pistons, *Proc. 1992 Coatings for Advanced Heat Engines Workshop,* U.S. Department of Energy, 1992, p II-31 to II-40
14. P.M. Pierz, Thermal Barrier Coating Development for Diesel Engine Aluminum Pistons, *Surf. Coat. Technol.,* Vol 61, 1993, p 60-66
15. M. Yamanouchi, M. Koizumi, T. Hirai, and I. Shiota, Ed., *Proc. First Int. Symp. Functionally Graded Materials,* FGM Forum, Japan, 1990
16. J.B. Holt, M. Koizumi, T. Hirai, and Z.A. Munir, Ed., *Functionally Gradient Materials,* Vol 34, *Ceram. Trans.,* American Ceramic Society, 1993
17. B.D. Choules and K. Kokini, Multilayer Ceramic Coating Architecture against Surface Thermal Fracture, *Proc. Symp. Ceramic Coatings,* K. Kokini, Ed., ASME MD, Vol 44, 1993, p 73-86